

# Electrochemical Characterization of Battery Materials in 2-Electrode Half-Cell Configuration: A Balancing Act Between Simplicity and Pitfalls

Christian Heubner,<sup>\*[a]</sup> Sebastian Maletti,<sup>[b]</sup> Oliver Lohrberg,<sup>[b]</sup> Tobias Lein,<sup>[b]</sup> Tobias Liebmann,<sup>[b]</sup> Alexander Nickol,<sup>[a]</sup> Michael Schneider,<sup>[a]</sup> and Alexander Michaelis<sup>[a, b]</sup>

The development of advanced battery materials requires fundamental research studies, particularly in terms of electrochemical performance. Most investigations on novel materials for Li- or Na-ion batteries are carried out in 2-electrode half-cells (2-EHC) using Li- or Na-metal as the negative electrode. Although such cells are easy to assemble and generally provide sufficient stability, scientists should be aware of any effects that may influence the measurements, and care should be taken when interpreting the corresponding results. The present work addresses specific effects that can affect the electrochemical response of measurements in 2-EHC. Critical points to be considered for long-term cycling tests and impedance analyses are discussed and illustrated with relevant examples. The

different behavior of electrochemically deposited and pristine alkali metal electrodes is shown, deriving the corresponding impact on the characterization of the actual material of interest. We demonstrate possible impacts of anode-cathode crosstalk effects on the evaluation of measurements in 2-EHC and highlight challenges and pitfalls in the interpretation of measurements in 2-EHC with respect to kinetic and thermodynamic properties and battery performance. These findings contribute to the understanding of the limitations of electrochemical characterization in 2-EHCs and should be carefully considered by researchers when evaluating novel battery materials.

## 1. Introduction

Li-ion batteries have been continuously improved over the last decades with the aim of extending the operating life of mobile electronic devices and realizing mass implementation in hybrid and all-electric vehicles.<sup>[1–4]</sup> However, user acceptance for automotive applications is still limited due to safety concerns, range limitations, and insufficient fast charging capability.<sup>[5–7]</sup> Academia and industry have evaluated various approaches to improve energy density at the cell level and have made continuous progress, such as the development of high-capacity anode<sup>[8,9]</sup> and cathode<sup>[10,11]</sup> materials, novel electrolytes,<sup>[12]</sup> improvements in electrode design<sup>[13,14]</sup> and composition<sup>[15–17]</sup> and the optimization of cell architecture.<sup>[18,19]</sup> In particular, it was found that the development of high-capacity electrode materials has by far the greatest potential for optimization.<sup>[20]</sup> Moreover, post-Li battery concepts, among which Na-ion batteries are particularly promising, are still in their infancy and

require intense development of active materials.<sup>[21]</sup> For this reason, basic research studies are necessary for testing and evaluating novel battery materials. This includes various electrochemical techniques<sup>[22]</sup> and cell types<sup>[23]</sup> capable to determine kinetic and thermodynamic parameters as well as properties relevant for battery application.

Most investigations on novel materials for Li- and Na-ion batteries are carried out in 2-electrode coin cells using Li- and Na-metal as the negative electrode, hence acting as counter and reference electrode. While these cells are easy to assemble and commonly provide sufficient stability, they exhibit several drawbacks, which may lead to errors and/or misinterpretations. The advantages and disadvantages of different cell configurations for the characterization of battery materials have recently been described in detail by Winter's group.<sup>[23]</sup> The authors discuss different arrangements used for the electrochemical characterization of battery materials and highlight advantages and limitations of the different configurations. They provide the reader with a clear and consequent notation of the different cell setups, including half-cells (2-EHC/3-EHC), symmetrical cells (2-ESC), and full-cells in either two-electrode (2-EFC) or three-electrode (3-EFC) configuration, as schematically depicted in Figure 1. Winter's group<sup>[23]</sup> also summarized challenges related to the use of 2-EHC with alkali metal counter electrodes (CE) for the investigation of battery materials. In these cells, only the cell voltage is controlled or measured, including the overpotential at the alkali metal electrode. This influences the exact monitoring or precise control of the potential-dependent lithiation behavior of the actual electrode material of interest at the working electrode (WE). Furthermore, the use of alkali

[a] Dr. C. Heubner, A. Nickol, Dr. M. Schneider, Prof. A. Michaelis  
Fraunhofer Institute for Ceramic Technologies and Systems IKTS  
Winterbergstraße 28, 01277 Dresden, Germany  
E-mail: christian.heubner@ikts.fraunhofer.de

[b] Dr. S. Maletti, O. Lohrberg, T. Lein, T. Liebmann, Prof. A. Michaelis  
Institute of Materials Science, TU Dresden  
01062 Dresden, Germany

 Supporting information for this article is available on the WWW under  
<https://doi.org/10.1002/batt.202100075>

 © 2021 The Authors. *Batteries & Supercaps* published by Wiley-VCH GmbH.  
This is an open access article under the terms of the Creative Commons Attribution License, which permits use, distribution and reproduction in any medium, provided the original work is properly cited.

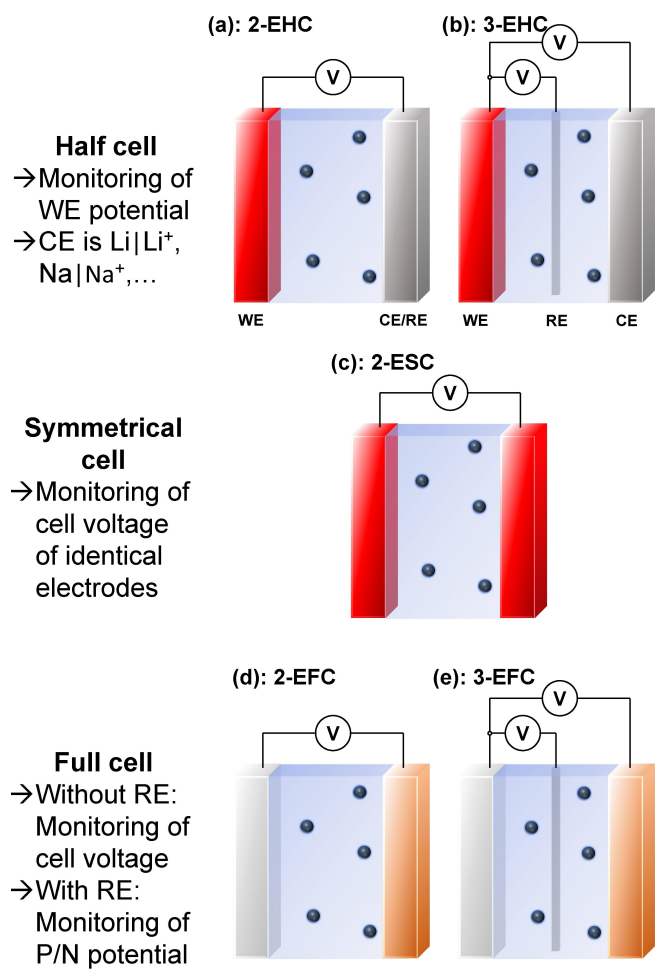


**Figure 1.** Types of cell setups: a) two-electrode half-cell (2-EHC) configuration with working electrode (WE) and a counter electrode (CE) that also serves as reference electrode (RE), b) three-electrode half-cell (3-EHC) configuration with separate reference electrode, c) symmetrical cell (2-ESC) consisting of two similar electrodes, d) two-electrode full-cell (2-EFC) configuration with positive (P) and negative (N) electrode, e) three-electrode full-cell (3-EFC) configuration with an additional RE. Adapted from Ref. [23] with permission.

metal electrodes results in a massive excess of Li or Na capacity, which affects the results compared to practical batteries with capacity-balanced electrodes. Winter's group<sup>[23]</sup> provide the reader with a guide to the correct choice of cell configuration suitable for the intended objective of the electrochemical study. Dugas et al. addressed the topic for the case of post-Li batteries (Na, K, Mg and Ca).<sup>[24]</sup> The authors emphasize the necessity of using a 3-EHC including a reference electrode (RE) for the investigation of novel battery materials with respect to material and electrode specific electrochemical properties (reversible capacity, Coulombic efficiency, material/electrode stability, etc.) in order to exclude influences of the CE. Raccichini et al. recently reviewed the state of the art in the application of REs in battery research.<sup>[25]</sup> It is concluded that, despite much progress in this field, a reliable, user-friendly, and completely artifact-free cell configuration with a chemically stable RE is not yet available.

Although the use of 3-EHCs provides several benefits intended to enable correct interpretation of the electrochemical response, unequivocal identification of the contribution of each cell component, and valid studies of reaction mechanisms, serious challenges exist regarding the chemical stability of the RE, as well as its location and geometry with respect to the other cell components. As a result, the vast majority of studies on electrode materials is being conducted using 2-EHC with alkali metal negative electrodes. Scientists should therefore be aware of the challenges and pitfalls associated with the use of 2-EHC to avoid misinterpretations and false conclusions regarding the electrochemical properties and performance metrics of novel battery materials. Besides the most obvious challenges, there are several effects that are much less understood or usually not considered in the characterization of battery materials in 2-EHC. Here we show such effects that can influence the electrochemical reactions, voltage profiles and obtained battery characteristics in 2-EHC. We discuss the impact of alkali metal CEs with respect to cycle life tests. Furthermore, we highlight critical points of impedance analyses in 2-EHC and illustrate these with corresponding examples. The different behavior of electrochemically deposited and pristine alkali metal at the counter electrode is shown and corresponding effects on the characterization of the actual material of interest are discussed. Possible effects of anode-cathode cross-talk on the evaluation of measurements in 2-EHC are shown. Finally, we discuss the main challenges and pitfalls when interpreting measurements in 2-EHC regarding kinetic and thermodynamic properties and battery performance and suggest straightforward approaches for checking interpretations and conclusions.

## 2. Results and Discussion

### 2.1. Challenges for Analyzing Cycling Stability in 2-EHCs

While improved metal anodes,<sup>[26–31]</sup> electrolytes<sup>[32,33]</sup> and advanced characterization methods to study metal deposition<sup>[34–38]</sup> are being developed in the context of Li- and Na-metal batteries, the use of non-optimized metal foils as CE in half-cells is a common practice in Li- and Na-ion battery research. In this regard, the most obvious but hardly considered problem with measurements in 2-EHC is the long-term behavior of the Li or Na CE. When performing long-term cycling tests in 2-EHC, researchers are commonly interested in the cycling stability of an active material or electrode connected as the WE. The cells are cycled in a defined voltage range until a lower threshold value of the discharge capacity is reached, e.g. 80% of the initial capacity. Based on the respective number of cycles achieved, the long-term stability of the active material or electrode of interest is evaluated. However, comparing typical results obtained in 2-EHCs and 2-EFCs with intercalation type electrodes indicates that the 2-EHCs do not necessarily reveal the stability of the material of interest. For example, Figure 2a compares the results of long-term cycling tests using a thick NMC622 (7 mAh cm<sup>-2</sup>) cathode in 2-EHC vs. Li-metal and in 2-

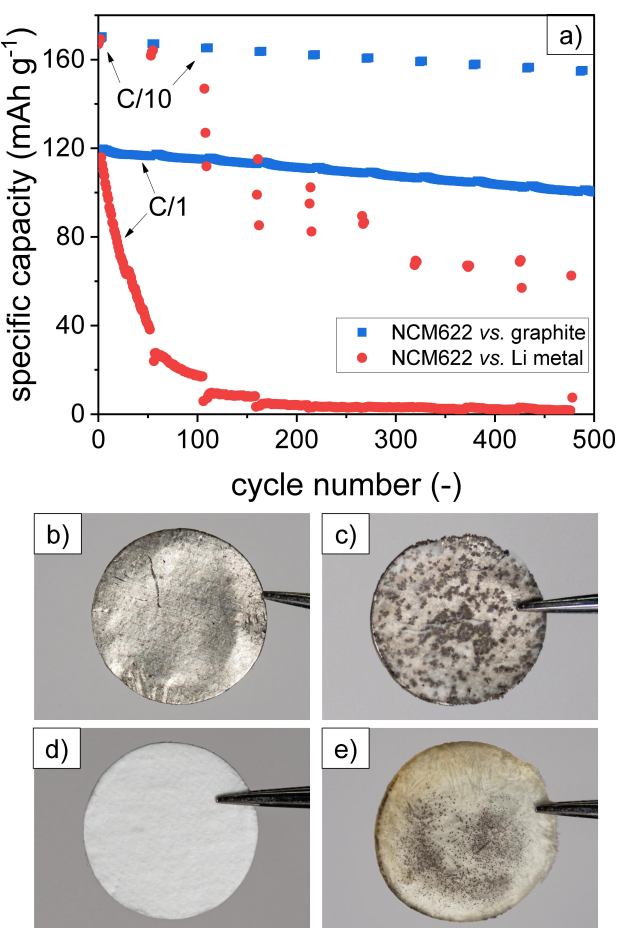


**Figure 2.** a) Comparison of long-term cycling tests of NCM622 cathodes carried out in 2-EHC against Li-metal and in 2-EFC against a graphite anode. Photographs comparing Li-metal CE (b,c) and glass fiber separator (d,e) in the pristine state (b,d) and after cycling (c,e).

EFC vs. graphite, respectively. The specific capacity with respect to the cathode material decreases slightly with increasing number of cycles in the case of the 2-EFC. In contrast, the cathode performance determined in 2-EHC is much worse with the specific capacity decreasing rapidly during the C/1 cycling phases. Post-mortem analysis reveals massive dendrite formation at the Li-metal electrode (Figure 2c). In the worst case, this leads to micro short circuits between the WE and CE, usually accompanied with noise in the voltage profile, resulting in reduced discharge capacity or even complete cell failure.<sup>[39,40]</sup> Furthermore, the dendrites block electrolyte transport through the separator (Figure 2e), which increases the internal resistance, again resulting in reduced cell performance. Accordingly, the analysis in 2-EHC does not give representative results regarding the electrochemical cycling performance of the actual material/electrode of interest. The formation of dendrites is particularly pronounced at high current densities, i.e., as present during cycling against cathodes with high areal capacity. For example, assuming an areal capacity of  $7 \text{ mAh cm}^{-2}$ , the C/1 cycling rate corresponds to a current density of  $7 \text{ mA cm}^{-2}$  at the Li-CE, which favors dendritic growth of Li.<sup>[41]</sup> In this context, it should be noted that the

dendrite growth through the separator is significantly influenced by its thickness, porosity and chemical nature.<sup>[42]</sup> The dendrite growth through a rather thick separator (e.g. 2x Whatman GF/C  $\sim 500 \mu\text{m}$  used here) takes longer than through a very thin separator (e.g. Celgard 2500  $\sim 25 \mu\text{m}$ ). Accordingly, these differences need to be considered when analyzing cycling data. Furthermore, it should be mentioned that the initial surface morphology of the metal electrode (before cycling) can also have a significant impact on the electrochemical performance. There are some examples of electrode processing that lead to improved long-term stability.<sup>[43,44]</sup> Another aspect that requires awareness is the electrolyte consumption of a Li metal counter electrode. Previous studies showed that thick Li foils consume large amounts of Li due to SEI formation and the subsequent cell failure could be misinterpreted as a bad cycling stability of the studied active material but is actually due to drying of the cell.<sup>[45]</sup>

In the present example (Figure 2), the electrochemical performance of the material of interest (NCM622) is underestimated when using 2-EHC. Similar observations have also been reported for sodium-ion batteries, in which a  $\text{Li}_4\text{Ti}_5\text{O}_{12}$  electrode showed a much faster capacity decay when combined with sodium metal rather than activated carbon counter electrodes.<sup>[46]</sup> Under certain circumstances, measurements in 2-EHC can also lead to an overestimation of the material or electrode performance. In particular, the use of alkali metals as the negative electrode represents a massive reservoir. Accordingly, insufficient Coulombic efficiency of the material or electrode of interest will not limit the cycling performance of the cell. In this case, a supposedly "excellent" cycle stability could be achieved in 2-EHC. However, a low Coulombic efficiency would lead to a dramatic capacity fade in full-cells. Theoretically, a Coulombic efficiency of 98% hardly affects the cycling performance in 2-EHC, since Li losses are compensated by the Li CE. On the other hand, in full-cell configuration against a practical anode, which does not provide excess Li, the capacity drops to 50% already after 35 cycles.<sup>[47]</sup> For example, in the case of Si anodes and NCM cathodes, high Coulombic efficiencies and stability were achieved in 2-EHC, respectively, while NCM//Si full cells showed an unexpectedly fast capacity drop due to the loss of cyclable Li.<sup>[48]</sup>

## 2.2. Challenges for Impedance Analyses in 2-EHCs

Electrochemical impedance spectroscopy (EIS) is one of the most powerful tools to characterize novel battery materials. The most common technique is to measure the impedance of a cell under an applied sinusoidal voltage with a low amplitude (5–10 mV versus open-circuit voltage) over a wide frequency range (typically  $10^{-2}$ – $10^5$  Hz). The impedance data are then analyzed by fitting the impedance response to an electrical equivalent circuit (EEC), representing the electrochemical reactions and transport processes in the cell. The importance and necessity of RE for impedance analysis, e.g., to increase reproducibility, has been highlighted in previous studies.<sup>[25,49–52]</sup> In the following, we extend the existing knowledge by

analyzing the quantitative influence of the Li metal counter electrode using simple equivalent circuit simulations and practical measurements at low temperatures as example to point out possible misinterpretations when using 2-EHCs.

Considering a 2-EHC, the impedance response includes the contributions of both, the CE and WE. While equivalent circuits that adequately reflect the behavior of the cell actually require transition line models, reaction schemes representing the porous electrode structure and a corresponding Poisson-Nernst-Planck framework,<sup>[53–56]</sup> simplified equivalent circuits are used by the vast majority of scientists to interpret impedance spectra.

Such a simplified EEC could be described as depicted in Figure 3a. Therein,  $R_\Omega$  represents the ohmic resistance of the cell.  $R_{sf,WE}$  and  $R_{sf,CE}$  represent surface film or contact resistances<sup>[57]</sup> and  $R_{ct,WE}$  and  $R_{ct,CE}$  are the charge transfer resistances of the WE and the CE, respectively, with the corresponding capacitances, C. The Warburg element, W, represents diffusion impedance at low frequency.

When analyzing 2-EHC, it is usually assumed that the impedance of the WE,  $Z_{WE}$ , is much larger than that of the CE,  $Z_{CE}$ . In this case the influence of the CE on the cell impedance could be neglected and the EEC could be simplified as depicted in Figure 3b. However, based on the impedance response of 2-EHC, it is often difficult to judge whether this assumption is correct. To illustrate this problem, Figure 3c shows simulated impedance spectra using the EEC shown in Figure 3a for different ratios  $Z_{WE}/Z_{CE}$  and the common fit applied when analyzing 2-EHCs (EEC Figure 3b). For  $Z_{WE} > Z_{CE}$ , the impedance spectrum measured in 2-EHC is quite similar to that of the WE. In this case, fitting the impedance data using the simplified EEC (Figure 3b) gives representative results regarding the properties

of the WE, e.g. charge transfer resistance. For  $Z_{WE} \sim Z_{CE}$ , the impedance spectrum measured in 2-EHC no longer represent the behavior of the WE and also no longer allow the differentiation of all electrode processes due to the overlapping of the different RC elements (similar time constants).

In this case, fitting the impedance data using the simplified EEC (Figure 3b) results in an overestimation of  $Z_{WE}$  and its individual contributions. For  $Z_{WE} < Z_{CE}$ , impedance spectrum measured in 2-EHC are close to those of the CE. Accordingly, fitting results obtained when using the simplified EEC (Figure 3b) do not reflect the properties of the WE, but the CE.

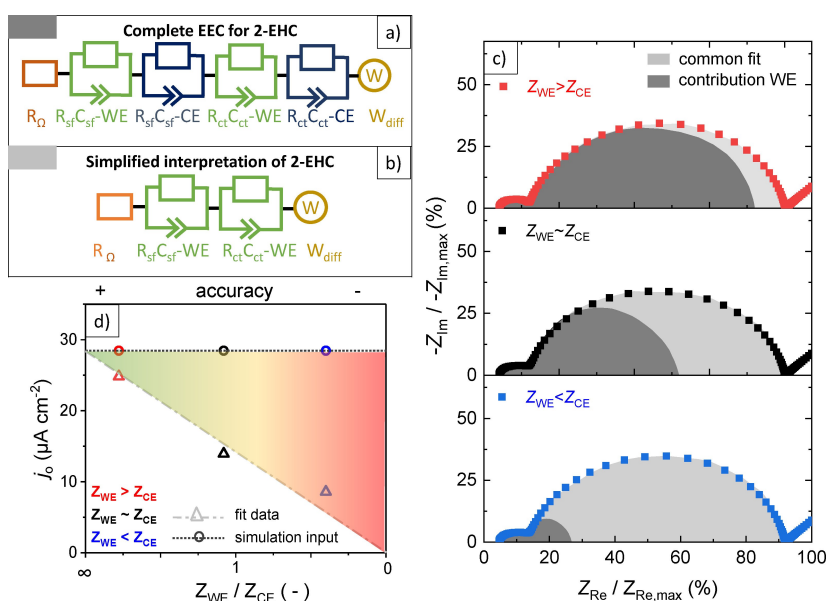
The greater the proportion of CE in the cell impedance, the greater the deviation resulting from a simplified fitting. Figure 3d compares the exchange current densities determined from fitting the impedance data in Figure 3c using the simplified EEC (Figure 3b) and the "true" values used for the simulation (see Table S1 for details). The exchange current density determined by fitting the data for  $Z_{WE} > Z_{CE}$  are close to the input parameters used for the simulations.

The results determined for  $Z_{WE} \sim Z_{CE}$  already show a significant deviation and for  $Z_{WE} < Z_{CE}$ , the fitted exchange current density is much lower than the input parameters used for the simulations.

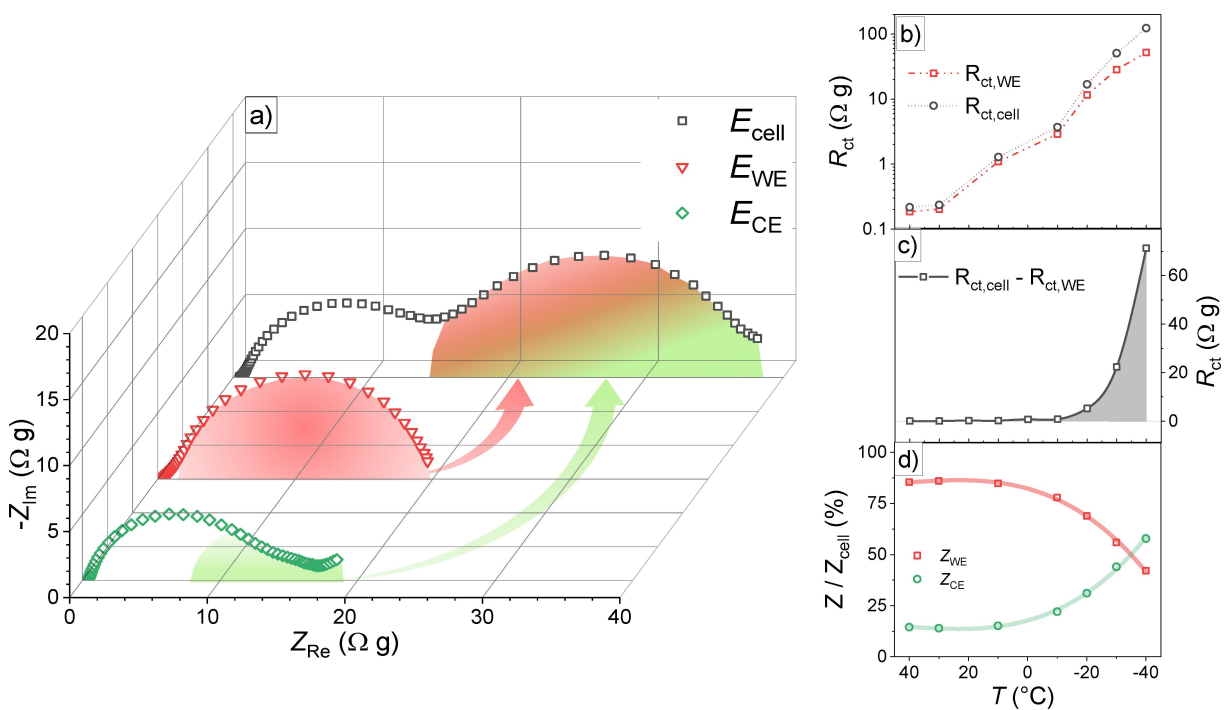
A practical example, where the impedance of the counter electrode cannot be neglected, is illustrated by means of impedance analyses of low temperature intercalation kinetics.

Figure 4a shows impedance spectra of an NCM523|Li|Li cell measured at  $-30^\circ\text{C}$  and SOC = 0.8.

In this case, the CE contributes significantly to the impedance in 2-EHC configuration ( $E_{cell}$ ). Furthermore, the overlapping of the processes at the CE and the WE does not allow assigning the individual contributions by means of fitting



**Figure 3.** Theoretical considerations of a) complete EEC representing the electrochemical processes inside a 2-EHC and b) commonly simplified interpretation neglecting the influence of the CE. c) Simulated impedance spectra with different contributions of  $Z_{WE}/Z_{CE}$ . The gray areas show the contribution of the WE and common fits (b) used to analyze impedance data obtained from 2-EHCs. d) Exchange current density determined from fitting the simulated impedance data using the simplified EEC (b) compared to the actual input data used for the simulation.



**Figure 4.** a) Impedance spectra of an NCM523 WE, Li-metal CE and corresponding 2-EHC data at  $-30^{\circ}\text{C}$  and SOC = 0.8. b) Temperature dependent charge transfer resistance determined in 2- and 3-EHC configuration. c) Error between charge transfer resistance obtained in 2- and 3-EHC configuration as a function of temperature and d) corresponding contributions of the WE and the CE to the 2-EHC impedance.

with a more complex EEC (e.g. Figure 3a). However, analyzing the data using the simplified EEC (Figure 3b) obviously yields falsified results concerning kinetic parameters, such as the charge transfer resistance, due to the impact of the CE (Figure 4b and 4c, see Table S2 for details).

While the influence of a Li CE might be neglected at room temperature if the impedance of the WE is sufficiently high, significant impact can be expected at low temperature. The increasing influence of the CE with decreasing temperature is shown in Figure 4d. While in this specific example the contribution of CE is low down to temperatures of  $-10^{\circ}\text{C}$ , it increases strongly at lower temperatures. At temperatures below  $-30^{\circ}\text{C}$ , it leads to CE dominating the spectrum. Thus, if the activation energies of the processes at the WE and CE differ significantly, the ratio of  $Z_{\text{WE}}/Z_{\text{CE}}$  depends on the temperature. Accordingly, the impedance of the cell might represent the behavior of the WE at room temperature but is dominated by the CE at lower temperatures. This can lead to falsification of the measurement results and corresponding conclusions regarding the kinetic properties of the investigated material or electrode.

### 2.3. Challenges Related to Electrodeposited Alkali Metal in 2-EHCs

During cycling of an arbitrary WE against an alkali metal CE, the pristine alkali metal is dissolved and redeposited. Thereby, a change in morphology takes place: while the pristine alkali metal is usually smooth (considering the use of a metal foil as

electrode), the electrodeposited metal grows non-uniform, often described as mossy or dendritic.<sup>[58]</sup> The electrodeposited alkali metal (ED-Li, ED-Na)<sup>[59]</sup> has much larger surface area than the pristine bulk material, being rich in defects and therefore lowering Li nucleation as well as dissolution overpotentials.<sup>[60]</sup> Moreover, effects of the solid electrolyte interphase (SEI) have to be considered. Li deposits, being in contact with electrolyte, exhibit a different surface film and therefore other Li<sup>+</sup> migration properties between solid and electrolyte than pristine Li metal.<sup>[61]</sup> In the following, we show with some illustrative examples how the different properties of electrodeposited and pristine alkali metal influence the behavior in 2-EHC and can lead to misinterpretations.

A first comprehensive example is given by an “anode-free” Li metal battery, where Li is plated *in situ* on a bare current collector.<sup>[47]</sup> Corresponding characterizations of novel current collector materials or electrolytes are commonly carried out using the respective current collector as WE and metallic Li as CE. Figure 5a displays the evolution of  $E_{\text{WE}}$  and  $E_{\text{CE}}$  versus a Li reference electrode, as well as the apparent potential difference between WE and CE,  $E_{\text{cell}}$ , corresponding to the voltage measured in a 2-EHC. Following  $E_{\text{cell}}$ , a continuous slope during Li plating would suggest a steady decrease of the WE potential and might be interpreted as a rise of overvoltage as the plating proceeds. A closer look at the actual electrode potentials clearly reveals, that this increase originates from the CE, while the WE shows a neglectable potential change in comparison. Figure 5b depicts a close-up on the first stripping and the second plating cycle. During plating,  $E_{\text{cell}}$  is initially approximately constant at  $-0.03\text{ V}$ , followed by a sloping region and another plateau at

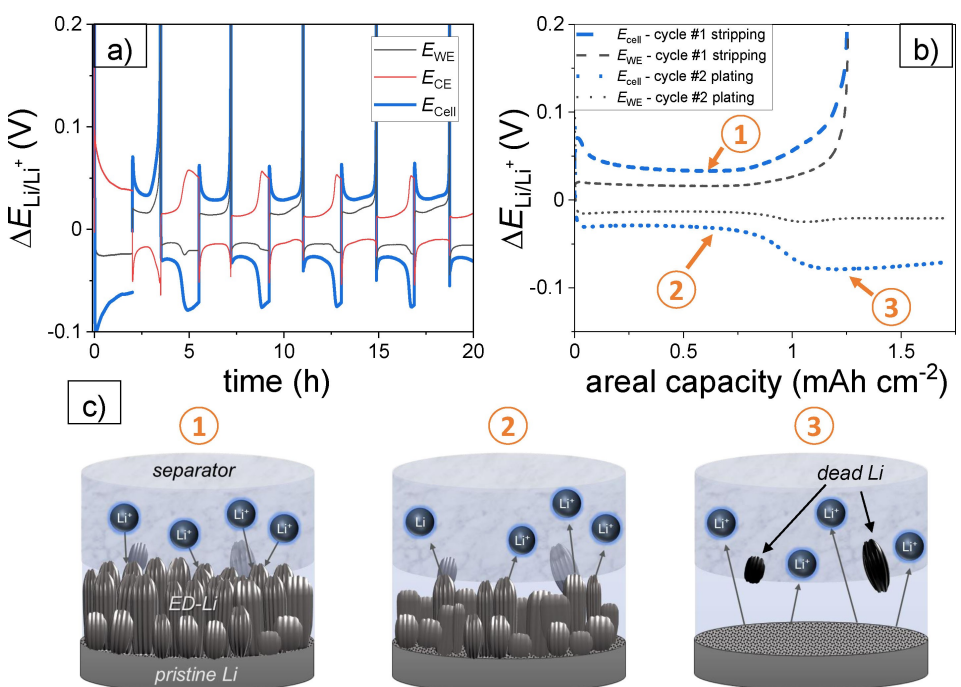


**Figure 5.** a) Evolution of the different half-cell potentials during the first five cycles in an “anode-free” cell configuration with WE: Cu foil, CE: Li, RE: Li, b) analysis of the first stripping and the second plating cycle, c) Scheme illustrating the mechanism of deposition and dissolution of ED–Li and pristine Li.

–0.07 V. Evidently,  $E_{\text{WE}}$  remains almost unchanged during the whole plating process and the measured change in  $E_{\text{cell}}$  arises from the CE. Comparing the preceding stripping cycle, the occurrence of the sloping region coincides with the amount of Li stripped from the WE (and therefore plated on the CE) previously. This behavior is interpreted as follows: First, during Li stripping at the WE, Li is deposited at the CE, see Figure 5c (1), forming a layer of ED–Li. During the subsequent half cycle, the ED–Li is dissolved at a low overpotential (2). A certain fraction of the ED–Li is thereby detached irrecoverably and ends up as “dead Li”, no longer taking part in the electrochemical processes.<sup>[62]</sup> The amount of dead Li generated each cycle needs to be replaced by pristine “bulk” Li.<sup>[63]</sup> As soon as the available ED–Li is consumed, an increase in overvoltage occurs, as from this point, the pristine Li needs to be dissolved (3), which further proceeds at a constant potential. Comparing the initial Li stripping at the CE (Figure 5a) confirms these assumptions, since, in this state, no ED–Li is present at all and pristine Li is dissolved from the beginning. This behavior could lead to serious misinterpretations when investigating a novel material or electrode in 2-EHC.

A second example, where the different behavior of ED–Li and pristine Li affects the analysis in 2-EHC, is taken from investigations of Si anodes (Figure 6). Already at 0.3 V (Figure 6a), the impedance spectrum obtained in 2-EHC does not represent the characteristics of the Si-anode, as it is mainly determined by the Li CE. Accordingly, analyzing the 2-EHC impedance data regarding kinetic parameters, e.g. exchange current density,<sup>[64]</sup> would lead to wrong results, as described above. Discharging the cell to 0.01 V doubles the impedance, when solely considering the 2-EHC (Figure 6b). Typically,

researchers assign changes in electrode properties with the lithiation state (SOC, electrode potential) to the electrode material under investigation. Consequently, this behavior could mistakenly lead to the conclusion that the impedance of Si WE has increased significantly. In fact, the impedance of the Si WE changes only slightly, while the main contribution originates from the Li CE, whose impedance more than doubles. This is caused by abovementioned different electrochemical behavior of ED–Li and pristine Li. During discharging of the Si|Li cell, pristine Li starts to dissolve after the available ED–Li from the previous charging is consumed. At this point, the impedance at the Li electrode rises, causing the larger impedance recorded in 2-EHC. A similar measurement, carried out in a coin cell, is shown in Figure S1, confirming a massive impedance rise at lower potential. In this case, the 2-EHC setup does not allow a differentiation between WE and CE contributions, misleading the experimenter to assign the whole impedance increase to Si as the electrode of interest.

A further example, where the behavior of the CE can significantly affect the electrochemical behavior of the cell voltage in 2-EHCs, is shown in Figure 7. Figure 7a depicts voltage profiles of a LiFePO<sub>4</sub>|Li|Li cell after repeated cycling. During charging, the typical LiFePO<sub>4</sub> (LFP) potential plateau is observed,<sup>[65]</sup> hardly differing for  $E_{\text{WE}}$  and  $E_{\text{cell}}$ . The voltage profile measured during discharging exhibits an additional plateau region around SOC=0.9, when considering  $E_{\text{cell}}$ . Closer inspection of  $E_{\text{WE}}$  and  $E_{\text{CE}}$  (Figure 7a bottom) reveals that the occurrence of the second plateau is caused by an increase in overpotential at the CE. According to the behavior described above, this can again be assigned to the transition between the dissolution of ED–Li (low overpotential) and pristine Li (high

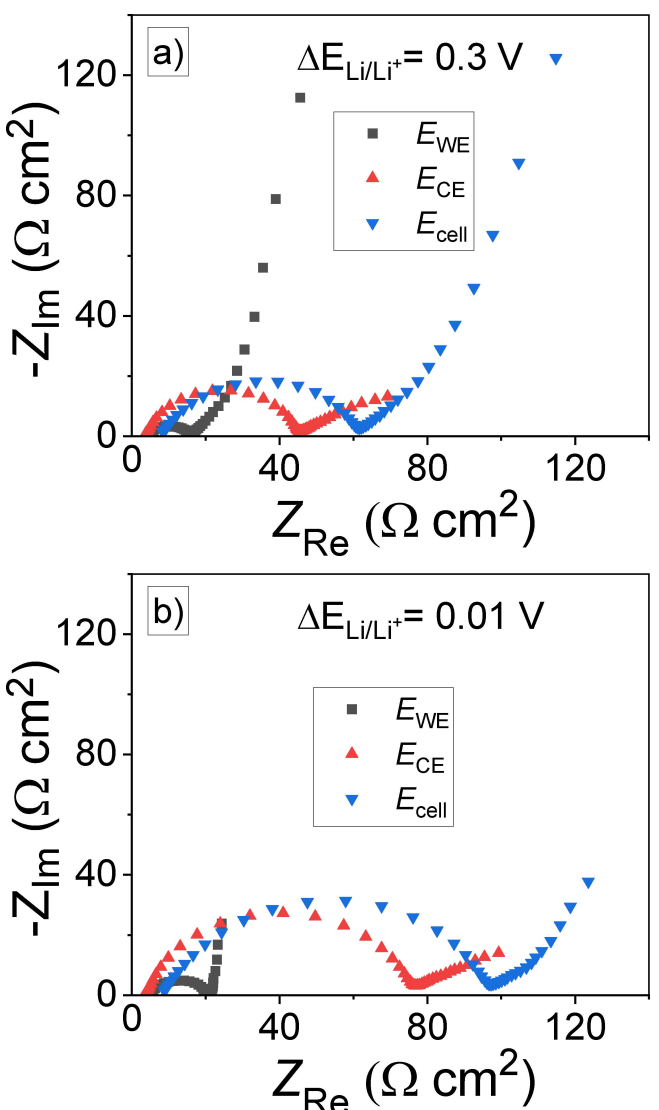


**Figure 6.** EIS analysis of a Si anode in 2-EHC against Li metal as counter and reference electrode. The spectra were obtained after discharging to a) 0.3 V and b) 0.01 V. The strong increase in impedance is mainly attributed to the counter electrode.

overpotential). Figure 7a indicates that this behavior hardly affects the capacity obtained from the WE. However, the changes at the Li CE distort the shape of voltage profile, which is of interest for several analytical approaches. Typically, thermodynamic investigations on battery materials include the analyses of potential profiles as they contain information on the phase transition behavior, ordering phenomena, etc., which were used to set up phase diagrams and support fundamental research based on first principles.<sup>[66–68]</sup> For example, if measured correctly, potential plateaus mark the stability range of two-phase regions, whereas sloping potential profiles indicate solid solution behavior. Furthermore, differential capacity analysis plays a key role in understanding degradation and capacity fading of batteries, supporting the development of tools for SOC and SOH estimation in practical devices.<sup>[69–71]</sup> Similarly, the evaluation of small voltage oscillations in galvanostatic charge/

discharge processes can be used for real-time analysis of phase separation dynamics in multiparticle electrodes.<sup>[72]</sup> Accordingly, deviations from the potential profile of the actually addressed material ( $E_{WE}$ ), due to the described influence of the negative electrode, can sabotage these works, leading to misinterpretations and misguided research approaches.

The behavior observed in 2-EHC employing Li-metal also occurs in the respective Na-counterparts. Figure 7b shows charge-discharge voltage profiles of a  $\text{NaFePO}_4\text{||Na}$  cell after repeated cycling. During charging, two potential plateaus are observed. The first one is related to a biphasic reaction between  $\text{NaFePO}_4$  and  $\text{Na}_{2/3}\text{FePO}_4$ , followed by a second biphasic reaction between  $\text{Na}_{2/3}\text{FePO}_4$  and  $\text{FePO}_4$ .<sup>[73,74]</sup> During discharging, also two potential plateaus are found, whereby the second plateau is only slightly intimated (marked with the circle). These observations suggest a reversible, path-independent phase transition behavior of  $\text{NaFePO}_4$  during charging and discharging. However, as known from comprehensive electrochemical studies including operando materials characterization, the phase transition behavior of  $\text{NaFePO}_4$  differs for charging and discharging.<sup>[75–79]</sup> As the cell mismatch between  $\text{NaFePO}_4$  and  $\text{Na}_{2/3}\text{FePO}_4$  is much lower than for  $\text{Na}_{2/3}\text{FePO}_4$  and  $\text{FePO}_4$ , the phase transformation behavior is asymmetrical, showing a single plateau during discharging (direct  $\text{FePO}_4$  to  $\text{NaFePO}_4$  conversion) and an intermediate phase ( $\text{Na}_{2/3}\text{FePO}_4$ ) during charging to buffer the lattice mismatch. The reason for the second voltage plateau observed during discharging in 2-EHC is again related to the CE (cf. Figure 7b bottom). Similar to the phenomenon in 2-EHC employing Li-metal, the overpotential required to drive Na-dissolution at the CE differ for the ED-Na and the pristine Na. Depending on the Coulombic efficiency of Na deposition/dissolution, pristine Na starts to dissolve at the end of each discharge cycle. As the deposition of the pristine alkali metal requires a higher overvoltage, the cell voltage in 2-EHC drops and forms a second plateau, which is, however, not related to any phase transitions at the WE. Like for LFP||Li cells, this can lead to serious misinterpretations and misconception of the battery performance of the actual material of interest.

#### 2.4. Challenges Related to Crosstalk Effects in 2-EHCs

During battery cycling, Li-ions are shuttled between the positive and negative electrode. Commonly, it is assumed that the full-cell response is given by the serial connection of the half-cell responses of anode and cathode. So-called crosstalk effects, in which one electrode influences the behavior of the other electrode, can however negate this assumption. For example, it is known that the electrochemical performance of NCA and NMC cathodes is worse with Li-metal anodes when compared with graphite or LTO anodes.<sup>[80,81]</sup> This is related to structural degradation,<sup>[82,83]</sup> but also cross-talk phenomena, where the SEI formed on the Li-metal anode is dissolved and migrates to the cathode side, affecting stability and interfacial kinetics.<sup>[84]</sup> Furthermore, the dissolution of transition metals (TM) from cathodes into electrolytes and the resulting TM-deposition on the anode surface is a well-known failure mode

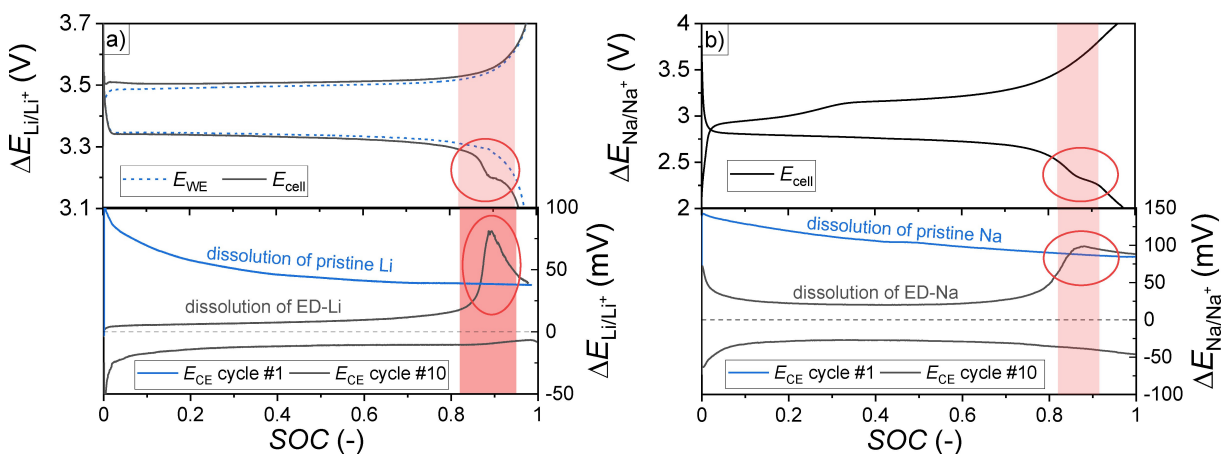


**Figure 7.** Charge-discharge voltage profiles of a)  $\text{Li}_{x}\text{FePO}_4 \mid \text{Li}$  half-cell (top) and b)  $\text{Na}_{x}\text{FePO}_4 \mid \text{Na}$  half-cell (top) and respective overpotential during galvanostatic a) Li, b) Na deposition (dashed lines) and dissolution (bottom). For comparison, the overpotential measured during the initial dissolution of Li and Na is shown. The circles mark the impact of Li and Na dissolution on the respective 2-EHC measurement.

of LIBs.<sup>[85–88]</sup> Placke and co-workers showed that the type of cathode material affects the deposition/dissolution behavior of a Li-metal anode due to crosstalk between cathode and anode by specific TM-dissolution behavior.<sup>[89]</sup> LNMO cathodes cause higher Li overpotentials and lead to a wider and more homogeneous distribution of Li deposits during the first deposition, while NMC622 and LFP cause spot like Li deposition. With ongoing cycling, nodule-like deposits emerge for NMC622 and LFP, whereas small spherical deposits are obtained using LNMO cathodes. The morphology affects the electrochemical behavior of the Li-metal anode and thus the cell voltage in 2-EHC, leading to misinterpretations concerning the behavior of the WE and the electrode material of interest. In addition to the type of active material, TM dissolution also depends on several other properties, in particular the degree of delithiation, which is influenced by the cut-off potential, and by the N:P ratio (areal capacity balance of negative (N) and positive (P) electrode). Furthermore, particle properties and the type of electrolyte significantly affect the dissolution/deposition behavior, as shown for NCM523 | graphite cells,<sup>[40,90]</sup> and thus have implications for corresponding cross-talk effects and electrochemical response in 2-EHCs. Another impressive but rarely considered example of crosstalk effects concerns the influence of current density distribution along the thickness of porous intercalation electrodes on the behavior of the CE.<sup>[91]</sup> This crosstalk between cathode and anode results from changes in the concentration gradient in the electrolyte, as illustrated in Figure 8. Depending on the position of the current density maximum in the porous WE, the Li concentration,  $c_{CE}$ , in front of the CE changes. For example, shifting the maximum of the local current density in the WE towards the back of the electrode, near the current collector, causes an increase of  $c_{CE}$ . Such shifts, sometimes also called current density waves, are typical for materials that undergo reversible phase transformations characterized by potential plateaus during intercalation and deintercalation, respectively.<sup>[92]</sup> According to the laws of Nernst and Butler-Volmer, both the potential and the overvoltage depend on the local concentration at the elec-

trode. Therefore, changes in the current density distribution in the porous WE cause changes of  $E_{cell}$  when using a 2-EHC, which are not exclusively related to the WE but also to the CE.

A representative example is depicted in Figure 8b by comparing the potential of a graphite WE and a respective 2-EHC, as a function of SOC during constant current lithiation. The typical plateau regions of graphite are observed, which are associated with phase transitions.<sup>[93,94]</sup> Two-phase regions are characterized by plateaus, whereas single-phase regions are assigned by inflection points in the potential curve.<sup>[66]</sup> The voltage measured in 2-EHC deviates from the potential of the graphite WE because the overpotential required to drive the Li deposition/dissolution at the CE adds to the cell voltage (Figure 8c). In contrast to the expected behavior during galvanostatic Li deposition/dissolution,  $E_{CE}$  shows characteristic features. These deviations from the expected potential transient are related to variations of  $c_{CE}$  caused by changes of the current density distribution along the thickness of the porous WE as schematically depicted in Figure 8a. In composite electrodes with negligible electron transport limitations, the transport of ions dominates the propagation of the lithiation front, while electrons move quickly from the current collector through the composite. Consequently, the lithiation of graphite electrodes starts near the separator and  $c_{CE}$  is relatively low (cf. Figure 8a).<sup>[95]</sup> Within the two-phase regions ( $E_{WE}$  plateaus), the reaction front shifts towards the current collector as the phase transition progresses. The extension of the effective diffusion path increases  $c_{CE}$  (cf. Figure 8a), causing an increase of  $E_{CE}$  (Figure 8c). In the following single-phase regions (sloping  $E_{CE}$ ), the local current density maximum is shifted back towards the separator. Accordingly,  $c_{CE}$  decreases again and the  $E_{CE}$  returns to the initial value.

Note that the final increase of  $E_{CE}$  during Li-dissolution (Figure 8c) is again related to the different behavior of ED-Li and pristine Li. The relationship between phase transition regions and changes of  $E_{CE}$  are particularly evident from Figures 8d and e, wherein  $E_{CE}$  is compared with the derivative  $dE/d\text{SOC}$ , with the latter being a sensitive indicator for phase

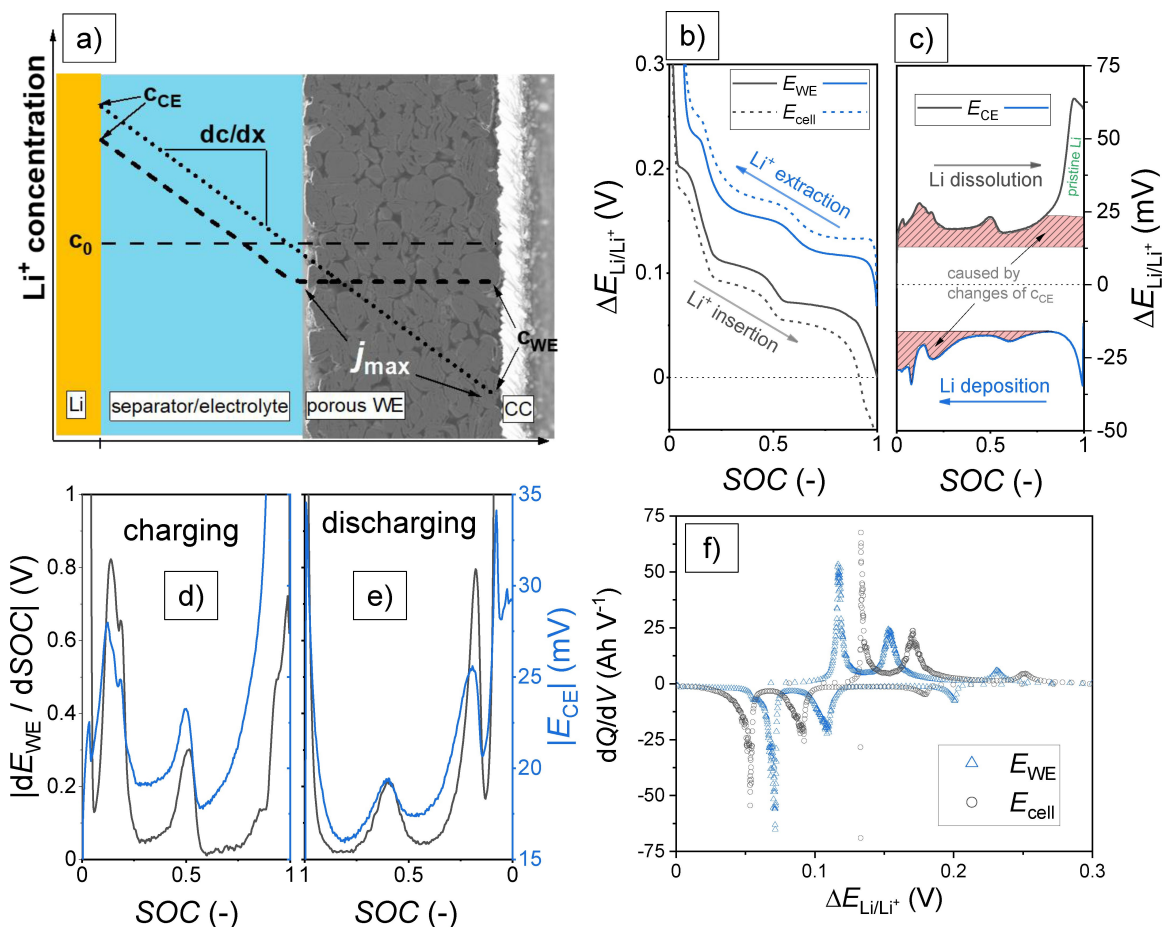


**Figure 8.** a) Scheme illustrating the relationship between the position of the local current density maximum,  $j_{\max}$ , in a porous WE and the electrolyte concentration in front of the CE. b) Potential profiles of a graphite electrode and a graphite|Li cell, and c) corresponding overpotential at the CE. d), e) Comparison of the derivative  $dE/dSOC$  and the overpotential at the CE. f) Differential capacity of a graphite electrode and a graphite|Li cell.

transitions of the WE.  $dE/dSOC$  displays two phase regions as a minimum, whereas single-phase regions occur as maxima. The clear accordance between the characteristic features of  $dE/dSOC$  and  $E_{CE}$  proves that the potential characteristics observed at the CE are in basic relationship to the lithiation/delithiation of graphite and the associated phase transitions. Furthermore, the interpretations agree with the behavior proposed by simulations of intercalation and relaxation in lithium-ion insertion cells<sup>[92]</sup> as well as experimental investigations of the current density distribution in porous electrodes.<sup>[96,97]</sup> Like the behavior observed for investigations on graphite anodes, measurements in 3-EHC of several different cathode materials show that  $E_{CE}$  is affected by the phase transitions of the WE.<sup>[89]</sup>

The impact of such crosstalk effects on the cell voltage in 2-EHC might be considered relatively small in most of the cases but might become significant for very thick electrodes and very high charge/discharge rates. In this case, analyses of the potential profile in view of differential capacity, phase transitions and degradation analysis can lead to misinterpretations if the impact of the counter electrode is not considered. For example, the increasing of  $E_{CE}$  during the progression of a two-phase reaction at the WE might affect the actual plateau character of the electrode material of interest, leading to wrong

conclusions about the phase transition behavior. Furthermore, the differential capacity is affected by the CE (Figure 8f), showing shifts and changes in the shape of characteristic peaks and the occurrence of additional features related to crosstalk effects.

### 3. Conclusions and Recommendations

Several effects occurring in 2-EHC with alkali metal negative electrodes can influence the electrochemical response but are not related to the actual material or electrode of interest. If not considered properly, this can lead to serious misinterpretations regarding the kinetic and thermodynamic properties and misjudgments of the battery performance. Generally, choosing an appropriate cell setup depends on the aim of the experimental study and the specific scientific question. When investigating novel battery materials, the application of 3-EHCs is highly recommended to exclude CE effects. Although the experimental effort is much higher and long-term stability as well as positioning of the RE are currently still sources of error, the advantages of 3-EHCs clearly outweigh 2-EHCs. However, due to its simplicity and

reproducibility (e.g. automated cell assembly), 2-EHCs with alkali metals as the negative electrode are the most commonly used arrangement in battery research and will most likely remain so in the future. Therefore, researchers should be aware of the effects occurring at 2-EHC and make additional efforts to verify their conclusions.

Investigations concerning the cycling stability of novel battery materials in 2-EHC can be sabotaged by the alkali metal CE in different ways. The cycle performance could be aggravated by increasing impedance of the CE, a blockage of the separator by dendritic alkali metal, or even a short circuit of the cell due to dendrite growth. On the other hand, the presence of excess alkali metal in the cell can lead to an overestimation of the cycling stability, e.g. if the Coulombic efficiency of the material of interest is insufficient. For investigations on the cycling stability in 2-EHC, additional Li|Li or Na|Na cells should be cycled using the same test protocols as the actual cell (identical electric charge transferred). This allows to observe the development of the overpotential, occurrence of short circuits, etc. related to the Li or Na negative electrode during the long-term experiment. This way, it is easier to judge whether the cell performance is limited by the alkali metal CE or the actual material/electrode of interest. Final assessment of the cycling stability should be made using full-cells without an excess of alkali metal, e.g. using a well-known and stable intercalation type electrode as the CE. For example, LFP-based cathodes or LTO-based anodes can offer a high stability and less side reactions with the electrolyte.

In the case of EIS analyses, the use of a RE (3-EHC) is particularly recommended. EIS analyses in 2-EHC provide limited information regarding the electrode that actually dominates the impedance of the cell. This can lead to misjudgments regarding SOC and temperature dependent kinetic properties and misconception of corresponding follow-up work (e.g. model based optimization), if the impedance results do not represent the actual material under investigation. Thus, additional symmetrical cells, each consisting of two electrodes of interest and two alkali metal electrodes, respectively, should also be examined under similar conditions. This allows to reveal which electrode dominates the impedance of the cell in 2-EHC. Symmetrical cells with alkali metal electrodes should be cycled several times to detect any changes in impedance or achieve steady state.

Investigations concerning electrochemical properties of novel materials in 2-EHC can be affected by the different behavior of pristine and electrodeposited alkali metal as well as cross-talk effects, falsifying kinetic and thermodynamic analyses. To minimize this effect, it is recommended to use very thin (e.g.  $< 10 \mu\text{m}$ ) WE coatings. This balances the typically large difference in the active surface area between the porous WE and the flat alkali metal CE. Accordingly, the impedance of the WE increases and dominates the cell behavior. Furthermore, the smaller the areal capacity of the WE, the lower the current density at the CE for a given C-rate ( $\text{h}^{-1}$ ) or specific current ( $\text{A g}^{-1}$ ). This reduces the tendency for dendrite growth, which increases long-term stability and reduces the probability of

short circuits. While very thin WE are very well suited for electrochemical material characterization, caution is required when investigating long-term cycling stability. Here, it is more appropriate to use designs that are close to the application to be able to evaluate the influence of the electrode design and composition as well as the significantly higher current densities under realistic conditions.

Ideally, appropriate analytical techniques should be used to complement the electrochemical investigation to minimize the risk of misinterpretation. For example, measurements can be combined with advanced analytical techniques to identify/quantify the amount of dead lithium. It should not go unnoticed that the type and geometry of the cell as well as temperature and applied pressure also have an influence on the electrochemical behavior and stability of the cell. While certain quantitative aspects may differ slightly depending on the cell type and geometry, the phenomena shown in this work, using the example of button cells and Swagelok cells, are present in every 2-EHC and should be taken into account to avoid misleading conclusions.

The presented insights into the challenges and pitfalls associated with the characterization of materials and electrodes in 2-EHC should help the battery community to avoid misinterpretation and enable appropriate choice of the cell configuration depending on the scientific question. This would also improve the comparability between independent research studies to allow more valid conclusions and identification of promising research trends.

## Experimental Section

### Cycling stability section

Polycrystalline NCM622 (BASF), Carbon black (Timcal Super P Li) and PVDF (Solef Solvay 5130) were dissolved in a weight ratio of 91.4/4.4/4.1 in NMP (Biesterfeld Chemiedistribution GmbH, 95%) and tape-casted on an Al foil yielding a mass loading of  $32.9 \text{ mg cm}^{-2}$  and an areal capacity of  $5 \text{ mAh cm}^{-2}$ . As anode, metallic Li (99.9% trace metals basis, MTI corp.) or graphite (Hitachi SMG-A5), coated in a 95.8/1/3.2 weight ratio with Carbon black and PVDF on Cu foil (N:P = 1.2), were used. Coin cells were fabricated using two sheets of a glass fiber separator (Whatman GF/C), soaked with 1.0 M LiPF<sub>6</sub> in EC:DEC 1:1 and tested in a multichannel battery tester (BasyTec, CTS). For cycle life tests, a test procedure, starting with three cycles at C/10 (17.5 mA g<sub>NCM622</sub><sup>-1</sup>), followed by 50 cycles at C/1 (175 mA g<sub>NCM622</sub><sup>-1</sup>) is repeated 10 times. In each case, at least three identical cells were tested to ensure statistical confidence of the results.

### Impedance analysis section

NCM523 electrodes (MTI corp., 45  $\mu\text{m}$  thickness,  $12 \text{ mg cm}^{-2}$  ( $1.8 \text{ mAh cm}^{-2}$ )), 15  $\mu\text{m}$  Al current collector) were used as cathodes and Li metal (Sigma Aldrich) as counter electrode (circular disk) and reference electrode (wire) in T-type Swagelok cells. A 1 M LiPF<sub>6</sub> solution in EC:DEC:DMC 1:1:1 (by volume) served as electrolyte and two glass fiber sheets (Whatman GF/C) as separator. The formation procedure consisted of one galvanostatic cycle at C/10 (15 mA g<sub>NCM523</sub><sup>-1</sup>) and two galvanostatic cycles at C/5 (30 mA g<sub>NCM523</sub><sup>-1</sup>) at 25 °C. Subsequently, EIS measurements were carried out at

different state of charge and different temperatures in a climate chamber (Memmert), using a p-p amplitude of 10 mV in a frequency range from 200 kHz to 5 mHz. All electrochemical tests were performed with a VMP3 potentiostat/galvanostat (Biologic Instruments).

### Pristine vs. electrodeposited metal section

**Anode-free cell tests:** For measurements in anode-free cells, Cu foil (Gould Electronics, 18 µm) was pre-treated by NaOH and H<sub>2</sub>SO<sub>4</sub> and modified by dip-coating into a 1 mM solution of AgNO<sub>3</sub> (Appli-Chem GmbH, 99.8%) in distilled water to create a lithophilic layer<sup>[98]</sup> and used as working electrode. Two layers of glass fiber separator (Whatman GF/C) were soaked with overall 120 µl of 1 M LiPF<sub>6</sub> in EC:DMC (1:1 v/v) as electrolyte. As the counter electrode, a circular Li foil (MaTeck, 99.8%, 1.27 cm<sup>2</sup>) was used. The reference electrode was introduced into the Swagelok®-type 3-electrode cell as a Li wire. Li was plated and stripped galvanostatically at a current density of 0.85 mA cm<sup>-2</sup> using a potentiostat (VMP3 Biologic Instruments).

**Li-Si tests.** Si electrodes (0.9 mg cm<sup>-2</sup>, 3.2 mAh cm<sup>-2</sup>, 10 µm Cu current collector, preparation reported elsewhere<sup>[99]</sup>) were investigated in a setup as described above. 20 wt% of fluoroethylene carbonate (AlfaAesar, 98%) was added to the electrolyte solution of 1 M LiPF<sub>6</sub> in EC:DMC (1:1 v/v). The electrodes were discharged and charged galvanostatically at a current density of at 0.1 C (360 mA g<sub>Si</sub><sup>-1</sup>) at 25 °C. Electrochemical impedance spectroscopy was carried out at various potentials in a frequency range of 10 mHz–100 kHz using a p-p amplitude of 5 mV.

**Li-LFP and Na-NFP tests.** LFP (Novarials), PVDF 5130 (Solvay) and carbon black (Super P, Imerys) were mixed in NMP (99.5%, GPR Rectapur®) in a 77/11.5/11.5 ratio and casted onto an Al foil (MTI corp.). For Li-ion batteries, the prepared electrodes were tested against Li metal CE (MaTeck, 99.8%) using 1 M LiPF<sub>6</sub> EC:DEC electrolyte. For Na-ion batteries, NaFePO<sub>4</sub> was prepared by electrochemical Li/Na exchange, using LiFePO<sub>4</sub> as the starting material.<sup>[100,101]</sup> Na-metal (99%, Alfa Aesar) was used as CE and a solution of NaPF<sub>6</sub> (> 99.9%, Sigma Aldrich) in EC:DEC 1:1 (both Sigma Aldrich) was used as electrolyte. Electrochemical tests were carried out in Swagelok® cells, using two glass microfiber filters (Whatman GF/C) as the separator, soaked with electrolyte. For Li-ion batteries, the measurements were carried out in 3-electrode arrangement using electrodes with a mass loading of 6.9 mg cm<sup>-2</sup> at a current of 0.16 mA cm<sup>-2</sup> (C/7), a Li-metal wire in between the separators as the RE. For Na-ion batteries, the measurements were carried out in 2-electrode arrangement using electrodes with a mass loading of 0.67 mg cm<sup>-2</sup> and a current of 5.52 µA cm<sup>-2</sup>, corresponding to C/20. In the lack of a well-functioning RE these measurements were complemented by similar studies using symmetrical Na|Na cells to isolate the impact of the Na-metal electrode on the electrochemical response in 2-EHCs. Galvanostatic experiments were performed using a C/20 current in the range of 2–4 V on a VMP3 potentiostat (Biologic instruments).

### Crosstalk section

Electrodes were prepared using graphite (SLP 10, Timcal), carbon black (Super P, Timcal) and binder (styrene butadiene rubber/sodium carboxymethyl cellulose 4.7:1) in a 94:2:4 weight ratio on a 10 µm Cu current collector. As both CE and RE, Li foil (MaTeck, 99.8%) was used, either as a circle disk of 1.27 cm<sup>2</sup> area (CE) or as a wire (RE). Two layers polypropylene nonwoven fabric (Viledon®, Freudenberg) soaked with 1 M LiPF<sub>6</sub> in EC:DEC 1:1 were used as the separator. Electrochemical measurements were carried out in

3-electrode Swagelok® cells, using a constant current procedure as formation and a subsequent cycling at a constant current of 0.4 mA cm<sup>-2</sup> in a potential range of 0–1 V.

### Acknowledgements

This work was supported by the German Federal Ministry of Education and Research (BMBF) in the framework of the project KaSiLi (Grant No. 03XP0254) and by the European Union and the Free State of Saxony through the European Development Fund (EFRE) in the framework of the project NaKaSub (Sächsische Aufbaubank, SAB Grant No. 100345904). C.H. and S.M contributed equally to this work. The authors are grateful to Sahin Cangaz, Thomas Abendroth, Susanne Dörfler, and Holger Althues (Fraunhofer IWS) for providing Si anodes and fruitful discussions. Support from Jann Seeba and Sebastian Reuber (Fraunhofer IKTS) by contributing NCM622 electrodes and cycling data in the framework of the HiLo Project supported by the BMBF (Grant No. 03XP0070B) is kindly acknowledged. Open access funding enabled and organized by Projekt DEAL.

### Conflict of Interest

The authors declare no conflict of interest.

**Keywords:** batteries • characterization • lithium • impedance • accuracy • two-electrode • cell

- [1] B. Scrosati, J. Garche, *J. Power Sources* **2010**, *195*, 2419.
- [2] V. Etacheri, R. Marom, R. Elazari, G. Salitra, D. Aurbach, *Energy Environ. Sci.* **2011**, *4*, 3243.
- [3] B. Scrosati, J. Hassoun, Y.-K. Sun, *Energy Environ. Sci.* **2011**, *4*, 3287.
- [4] J.-M. Tarascon, M. Armand, *Nature* **2001**, *414*, 359.
- [5] D. Andre, S.-J. Kim, P. Lamp, S. F. Lux, F. Maglia, O. Paschos, B. Stiaszny, *J. Mater. Chem. A* **2015**, *3*, 6709.
- [6] R. Schmuck, R. Wagner, G. Höpzel, T. Placke, M. Winter, *Nat. Energy* **2018**, *3*, 267.
- [7] Y. Ding, Z. P. Cano, A. Yu, J. Lu, Z. Chen, *Electrochim. Energy Rev.* **2019**, *2*, 1.
- [8] S. Goriparti, E. Miele, F. de Angelis, E. Di Fabrizio, R. Proietti Zaccaria, C. Capiglia, *J. Power Sources* **2014**, *257*, 421.
- [9] W.-J. Zhang, *J. Power Sources* **2011**, *196*, 13.
- [10] N. Nitta, F. Wu, J. T. Lee, G. Yushin, *Mater. Today* **2015**, *18*, 252.
- [11] R. Marom, S. F. Amalraj, N. Leifer, D. Jacob, D. Aurbach, *J. Mater. Chem.* **2011**, *21*, 9938.
- [12] E. R. Logan, J. R. Dahn, *Trends Chem.* **2020**, *2*, 354.
- [13] S. De, P. W. Northrop, V. Ramadesigan, V. R. Subramanian, *J. Power Sources* **2013**, *227*, 161.
- [14] J. Ye, A. C. Baumgaertel, Y. M. Wang, J. Biener, M. M. Biener, *ACS Nano* **2015**, *9*, 2194.
- [15] C. Heubner, T. Liebmann, M. Schneider, A. Michaelis, *Electrochim. Acta* **2018**, *269*, 745.
- [16] S. Luo, K. Wang, J. Wang, K. Jiang, Q. Li, S. Fan, *Adv. Mater.* **2012**, *24*, 2294.
- [17] G. Liu, S. Xun, N. Vukmirovic, X. Song, P. Olalde-Velasco, H. Zheng, V. S. Battaglia, L. Wang, W. Yang, *Adv. Mater.* **2011**, *23*, 4679.
- [18] M. Roberts, P. Johns, J. Owen, D. Brandell, K. Edstrom, G. El Enany, C. Guery, D. Golodnitsky, M. Lacey, C. Lecoer, H. Mazor, E. Peled, E. Perre, M. M. Shajumon, P. Simon, P.-L. Taberna, *J. Mater. Chem.* **2011**, *21*, 9876.

- [19] T. S. Arthur, D. J. Bates, N. Cirigliano, D. C. Johnson, P. Malati, J. M. Mosby, E. Perre, M. T. Rawls, A. L. Prieto, B. Dunn, *MRS Bull.* **2011**, *36*, 523.
- [20] C. Heubner, S. Reuber, J. Seeba, P. Marcinkowski, K. Nikolowski, M. Schneider, M. Wolter, A. Michaelis, *J. Power Sources* **2020**, *479*, 228704.
- [21] Q. Liu, Z. Hu, M. Chen, C. Zou, H. Jin, S. Wang, S.-L. Chou, Y. Liu, S.-X. Dou, *Adv. Funct. Mater.* **2020**, *30*, 1909530.
- [22] X. Yang, A. L. Rogach, *Adv. Energy Mater.* **2019**, *9*, 1900747.
- [23] R. Nölle, K. Beltrop, F. Holtstiege, J. Kasnatscheew, T. Placke, M. Winter, *Mater. Today* **2020**, *32*, 131.
- [24] R. Dugas, J. D. Forero-Saboya, A. Ponrouch, *Chem. Mater.* **2019**, *31*, 8613.
- [25] R. Raccichini, M. Amores, G. Hinds, *Batteries* **2019**, *5*, 12.
- [26] E. Matios, H. Wang, C. Wang, W. Li, *Ind. Eng. Chem. Res.* **2019**, *58*, 9758.
- [27] X.-B. Cheng, R. Zhang, C.-Z. Zhao, Q. Zhang, *Chem. Rev.* **2017**, *117*, 10403.
- [28] Y. Wang, Y. Wang, Y.-X. Wang, X. Feng, W. Chen, X. Ai, H. Yang, Y. Cao, *Chem* **2019**, *5*, 2547.
- [29] X. Zheng, C. Bommier, W. Luo, L. Jiang, Y. Hao, Y. Huang, *Energy Storage Mater.* **2019**, *16*, 6.
- [30] P. Shi, X.-Q. Zhang, X. Shen, R. Zhang, H. Liu, Q. Zhang, *Adv. Mater.* **2020**, *5*, 1900806.
- [31] H. Wang, E. Matios, J. Luo, W. Li, *Chem. Soc. Rev.* **2020**, *49*, 3783.
- [32] L. Fan, X. Li, *Nano Energy* **2018**, *53*, 630.
- [33] S. Li, Z. Luo, L. Li, J. Hu, G. Zou, H. Hou, X. Ji, *Energy Storage Mater.* **2020**, *32*, 306.
- [34] S. Drvarič Talian, J. Bobnar, A. R. Sinigoj, I. Humar, M. Gaberšček, *J. Phys. Chem. C* **2019**, *123*, 27997.
- [35] W. Liu, P. Liu, D. Mitlin, *Adv. Energy Mater.* **2020**, *10*, 2002297.
- [36] Y. Ma, S. Li, B. Wei, *Nanoscale* **2019**, *11*, 20429.
- [37] D. Liu, Z. Shadike, R. Lin, K. Qian, H. Li, K. Li, S. Wang, Q. Yu, M. Liu, S. Ganapathy, X. Qin, Q.-H. Yang, M. Wagemaker, F. Kang, X.-Q. Yang, B. Li, *Adv. Mater.* **2019**, *31*, e1806620.
- [38] P. P. Paul, E. J. McShane, A. M. Colclasure, N. Balsara, D. E. Brown, C. Cao, B.-R. Chen, P. R. Chinnam, Y. Cui, E. J. Dufek, D. P. Finegan, S. Gillard, W. Huang, Z. M. Konz, R. Kostecki, F. Liu, S. Lubner, R. Prasher, M. B. Peefer, J. Qian, M.-T. F. Rodrigues, M. Schnabel, S.-B. Son, V. Srinivasan, H.-G. Steinrück, T. R. Tanim, M. F. Toney, W. Tong, F. Usseglio-Viretta, J. Wan, M. Yusuf, B. D. McCloskey, J. Nelson Weker, *Adv. Energy Mater.* **2021**.
- [39] G. Homann, L. Stoltz, M. Winter, J. Kasnatscheew, *iScience* **2020**, *23*, 101225.
- [40] S. Klein, P. Bärmann, T. Beuse, K. Borzutzki, J. E. Frerichs, J. Kasnatscheew, M. Winter, T. Placke, *ChemSusChem* **2021**, *14*, 595.
- [41] P. Bai, J. Li, F. R. Brushett, M. Z. Bazant, *Energy Environ. Sci.* **2016**, *9*, 3221.
- [42] K. Liu, D. Zhuo, H.-W. Lee, W. Liu, D. Lin, Y. Lu, Y. Cui, *Adv. Mater.* **2017**, *29*.
- [43] J. Becking, A. Gröbmeyer, M. Kolek, U. Rodehorst, S. Schulze, M. Winter, P. Bieker, M. C. Stan, *Adv. Mater. Interfaces* **2017**, *4*, 1700166.
- [44] C. Yan, X.-B. Cheng, Y. Tian, X. Chen, X.-Q. Zhang, W.-J. Li, J.-Q. Huang, Q. Zhang, *Adv. Mater.* **2018**, *30*, e1707629.
- [45] J. Liu, Z. Bao, Y. Cui, E. J. Dufek, J. B. Goodenough, P. Khalifah, Q. Li, B. Y. Liaw, P. Liu, A. Manthiram, Meng, Y. Shirley, V. R. Subramanian, M. F. Toney, V. V. Viswanathan, M. S. Whittingham, J. Xiao, W. Xu, J. Yang, X.-Q. Yang, J.-G. Zhang, *Nat. Energy* **2019**, *4*, 180.
- [46] K. Pfeifer, S. Arnold, J. Becherer, C. Das, J. Maibach, H. Ehrenberg, S. Dsoke, *ChemSusChem* **2019**, *12*, 3312.
- [47] S. Nanda, A. Gupta, A. Manthiram, *Adv. Energy Mater.* **2020**, *6*, 2000804.
- [48] N. Dupré, P. Moreau, E. de Vito, L. Quazuguel, M. Boniface, A. Bordes, C. Rudisch, P. Bayle-Guillemaud, D. Guyomard, *Chem. Mater.* **2016**, *28*, 2557.
- [49] J. Landesfeind, D. Pritzl, H. A. Gasteiger, *J. Electrochem. Soc.* **2017**, *164*, A1773-A1783.
- [50] J. Costard, M. Ender, M. Weiss, E. Ivers-Tiffée, *J. Electrochem. Soc.* **2017**, *164*, A80-A87.
- [51] M. Ender, J. Illig, E. Ivers-Tiffée, *J. Electrochem. Soc.* **2017**, *164*, A71-A79.
- [52] D. Pritzl, J. Landesfeind, S. Solchenbach, H. A. Gasteiger, *J. Electrochem. Soc.* **2018**, *165*, A2145-A2153.
- [53] J. Moškon, J. Žuntar, S. Drvarič Talian, R. Dominko, M. Gaberšček, *J. Electrochem. Soc.* **2020**, *167*, 140539.
- [54] J. Moškon, M. Gaberšček, *J. Power Sources Adv.* **2021**, *7*, 100047.
- [55] S. Drvarič Talian, J. Bobnar, A. R. Sinigoj, I. Humar, M. Gaberšček, *J. Phys. Chem. C* **2019**, *123*, 27997.
- [56] N. Meddings, M. Heinrich, F. Overney, J.-S. Lee, V. Ruiz, E. Napolitano, S. Seitz, G. Hinds, R. Raccichini, M. Gaberšček, J. Park, *J. Power Sources* **2020**, *480*, 228742.
- [57] M. Gaberšček, J. Moškon, B. Erjavec, R. Dominko, J. Jamnik, *Electrochim. Solid-State Lett.* **2008**, *11*, A170-A174.
- [58] H. Liu, X.-B. Cheng, Z. Jin, R. Zhang, G. Wang, L.-Q. Chen, Q.-B. Liu, J.-Q. Huang, Q. Zhang, *EnergyChem* **2019**, *1*, 100003.
- [59] X. Wang, M. Zhang, J. Alvarado, S. Wang, M. Sina, B. Lu, J. Bouwer, W. Xu, J. Xiao, J.-G. Zhang, J. Liu, Y. S. Meng, *Nano Lett.* **2017**, *17*, 7606.
- [60] K. S. Nagy, S. Kazemiabnavi, K. Thornton, D. J. Siegel, *ACS Appl. Mater. Interfaces* **2019**, *11*, 7954.
- [61] F. Shi, A. Pei, D. T. Boyle, J. Xie, X. Yu, X. Zhang, Y. Cui, *Proc. Natl. Acad. Sci. USA* **2018**, *115*, 8529.
- [62] M. Arakawa, S. Tobishima, Y. Nemoto, M. Ichimura, J. Yamaki, *13th International Meeting on Lithium Batteries* **1993**, *43*, 27.
- [63] H. Liu, X.-B. Cheng, R. Xu, X.-Q. Zhang, C. Yan, J.-Q. Huang, Q. Zhang, *Adv. Energy Mater.* **2019**, *9*, 1902254.
- [64] C. Heubner, M. Schneider, A. Michaelis, *J. Power Sources* **2015**, *288*, 115.
- [65] A. K. Padhi, K. S. Nanjundaswamy, J. B. Goodenough, *J. Electrochem. Soc.* **1997**, *144*, 1188.
- [66] G. Ceder, A. Van der Ven, *Electrochim. Acta* **1999**, *45*, 131.
- [67] D. Li, H. Zhou, *Mater. Today* **2014**, *17*, 451.
- [68] A. L. Santhosha, L. Medenbach, J. R. Buchheim, P. Adelhelm, *Batteries & Supercaps* **2019**, *2*, 524.
- [69] H. M. Dahn, A. J. Smith, J. C. Burns, D. A. Stevens, J. R. Dahn, *J. Electrochem. Soc.* **2012**, *159*, A1405-A1409.
- [70] S. Torai, M. Nakagomi, S. Yoshitake, S. Yamaguchi, N. Oyama, *J. Power Sources* **2016**, *306*, 62.
- [71] L. Zheng, J. Zhu, D.-C. Lu, G. Wang, T. He, *Energy* **2018**, *150*, 759.
- [72] D. Li, Y. Sun, Z. Yang, L. Gu, Y. Chen, H. Zhou, *Joule* **2018**, *2*, 1265.
- [73] P. Moreau, D. Guyomard, J. Gaubicher, F. Boucher, *Chem. Mater.* **2010**, *22*, 4126-4128.
- [74] M. Casas-Cabanas, V. V. Roddatis, D. Saurel, P. Kubiak, J. Carretero-González, V. Palomares, P. Serras, T. Rojo, *J. Mater. Chem.* **2012**, *22*, 17421.
- [75] M. Galceran, D. Saurel, B. Acebedo, V. V. Roddatis, E. Martin, T. Rojo, M. Casas-Cabanas, *Phys. Chem. Chem. Phys.* **2014**, *16*, 8837.
- [76] J. Gaubicher, F. Boucher, P. Moreau, M. Cuisinier, P. Soudan, E. Elkaim, D. Guyomard, *Electrochim. Commun.* **2014**, *38*, 104.
- [77] D. Saurel, M. Galceran, M. Reynaud, H. Anne, M. Casas-Cabanas, *Int. J. Energy Res.* **2018**, *42*, 3258.
- [78] F. Boucher, J. Gaubicher, M. Cuisinier, D. Guyomard, P. Moreau, J. Am. Chem. Soc. **2014**, *136*, 9144.
- [79] M. Galceran, V. Roddatis, F. J. Zúñiga, J. M. Pérez-Mato, B. Acebedo, R. Arenal, I. Peral, T. Rojo, M. Casas-Cabanas, *Chem. Mater.* **2014**, *26*, 3289.
- [80] E. Björklund, D. Brandell, M. Hahlin, K. Edström, R. Younesi, *J. Electrochem. Soc.* **2017**, *164*, A3054-A3059.
- [81] H. Xiang, P. Shi, P. Bhattacharya, X. Chen, D. Mei, M. E. Bowden, J. Zheng, J.-G. Zhang, W. Xu, *13th International Meeting on Lithium Batteries* **2016**, *318*, 170.
- [82] H.-H. Ryu, K.-J. Park, C. S. Yoon, Y.-K. Sun, *Chem. Mater.* **2018**, *30*, 1155.
- [83] P. Yan, J. Zheng, M. Gu, J. Xiao, J.-G. Zhang, C.-M. Wang, *Nat. Commun.* **2017**, *8*, 14101.
- [84] H. Lee, H.-S. Lim, X. Ren, L. Yu, M. H. Engelhard, K. S. Han, J. Lee, H.-T. Kim, J. Xiao, J. Liu, W. Xu, J.-G. Zhang, *ACS Energy Lett.* **2018**, *3*, 2921.
- [85] I. A. Shkrob, A. J. Kropf, T. W. Marin, Y. Li, O. G. Poluektov, J. Niklas, D. P. Abraham, *J. Phys. Chem. C* **2014**, *118*, 24335.
- [86] M. M. Thackeray, *Prog. Solid State Chem.* **1997**, *25*, 1.
- [87] J. Vetter, P. Novák, M. R. Wagner, C. Veit, K.-C. Möller, J. O. Besenhard, M. Winter, M. Wohlfahrt-Mehrens, C. Vogler, A. Hammouche, *J. Power Sources* **2005**, *147*, 269.
- [88] I. Buchberger, S. Seidlmaier, A. Pokharel, M. Piana, J. Hattendorff, P. Kudejova, R. Gilles, H. A. Gasteiger, *J. Electrochim. Soc.* **2015**, *162*, A2737-A2746.
- [89] J. Betz, J.-P. Brinkmann, R. Nölle, C. Lürenbaum, M. Kolek, M. C. Stan, M. Winter, T. Placke, *Adv. Energy Mater.* **2019**, *9*, 1900574.
- [90] S. Klein, S. van Wickeren, S. Röser, P. Bärmann, K. Borzutzki, B. Heidrich, M. Börner, M. Winter, T. Placke, J. Kasnatscheew, *Adv. Energy Mater.* **2021**.
- [91] C. Heubner, U. Langlotz, M. Schneider, A. Michaelis, *J. Electroanal. Chem.* **2015**, *759*, Part 2, 91.
- [92] T. F. Fuller, M. Doyle, J. Newman, *J. Electrochim. Soc.* **1994**, *141*, 982.

- [93] A. Funabiki, M. Inaba, T. Abe, Z. Ogumi, *J. Electrochem. Soc.* **1999**, *146*, 2443.
- [94] J. R. Dahn, *Phys. Rev. B* **1991**, *44*, 9170.
- [95] Z. Chen, D. L. Danilov, R.-A. Eichel, P. H. Notten, *Electrochem. Commun.* **2020**, *121*, 106865.
- [96] S.-H. Ng, F. La Mantia, P. Novák, *Angew. Chem. Int. Ed.* **2009**, *48*, 528.
- [97] S. Klink, W. Schuhmann, F. La Mantia, *ChemSusChem* **2014**, *7*, 2159.
- [98] S. Cui, P. Zhai, W. Yang, Y. Wei, J. Xiao, L. Deng, Y. Gong, *Small* **2020**, *16*, e1905620.
- [99] M. Piwko, T. Kuntze, S. Winkler, S. Straach, P. Härtel, H. Althues, S. Kaskel, *J. Power Sources* **2017**, *351*, 183.
- [100] C. Heubner, T. Lein, M. Schneider, A. Michaelis, *J. Mater. Chem. A* **2020**, *8*, 16854.
- [101] C. Heubner, S. Heiden, M. Schneider, A. Michaelis, *Electrochim. Acta* **2017**, *233*, 78.

---

Manuscript received: March 29, 2021

Revised manuscript received: April 12, 2021

Accepted manuscript online: April 12, 2021

Version of record online: May 3, 2021

---